

Interpretations of High-Order Transient Absorption Spectroscopies

Peter A. Rose[†] and Jacob J. Krich^{*,†,‡}

[†]*Department of Physics, University of Ottawa, Ottawa, ON K1H 6N5, Canada*

[‡]*School of Electrical Engineering and Computer Science, University of Ottawa, Ottawa, ON K1H 6N5, Canada*

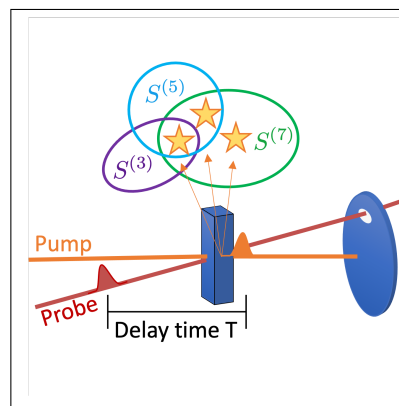
E-mail: jkrich@uottawa.ca

Abstract

Transient absorption (TA) spectroscopy has long been an invaluable tool for determining the energetics and dynamics of excited states in atomic, molecular, and solid-state systems. When pump pulse intensities are sufficiently high, the resulting TA spectra include both the generally desired third-order response of the studied material as well as responses that are higher order in the electric field amplitudes of the pulses. It has recently been shown that pump-intensity-dependent TA measurements allow separating the various orders of response of the TA signal, but the information content available in those higher orders has not been described. We give a general framework, intuition, and nomenclature for understanding the information contained in high-order TA spectra. Standard TA spectra are generally interpreted in terms of three fundamental processes: ground-state bleach (GSB), stimulated emission (SE), and excited state absorption (ESA), and we extend those concepts to higher order. Each order introduces two new processes: SE and ESA from highly excited states that were not accessible in lower orders. In addition, each order contains negations of lower-order processes, just as GSB is a negation of the linear absorption. We show the new spectral and dynamical information that is introduced at each order and show how the relative signs of the signals in different orders can

be used to identify which processes are dominant.

TOC Graphic



New forms of spectroscopy give new insights into the properties and dynamics of systems from atoms to solids. Linear absorption spectroscopy, in frequency ranges from THz to x-ray, gives information about the ground or thermal states of a material and its optically accessible excited states. Transient absorption (TA) spectroscopy measures the change in a probe pulse's absorption spectrum when it arrives a time T after a pump pulse, revealing both the absorption and dynamics of excited states¹⁻¹². The recently developed high-order transient absorption (HOTA) spectroscopy extends TA spectroscopy by systematically separating higher orders of nonlinear response, which has not previously been possible using TA methods¹³⁻¹⁵. These higher orders of nonlinear response contain both spectral and dynamical information about multiply excited states.

TA signals with pump pulses that are not too strong can be intuitively understood in terms of three fundamental processes: excited state absorption (ESA), stimulated emission (SE), and ground state bleach (GSB)¹⁶. There is a small probability that the pump excites the system into any of the available single-excitation states, which then evolve in time. When the probe arrives, the singly excited populations can either undergo SE back to the ground state or ESA up to doubly excited states. The population in the excited state is associated with a reduced population in the ground state, producing the GSB, which is a reduction of the linear absorption from the level without the pump.

The TA signal $S(T, \omega)$ gives the change in absorption of a probe pulse at frequency ω , which depends on the intensity of the pulses. Taking the electric dipole approximation and treating the fields classically, the standard interaction Hamiltonian is $H'(t) = -\boldsymbol{\mu} \cdot \mathbf{E}(t)$, where $\mathbf{E}(t) = \mathbf{E}_a(t) + \mathbf{E}_b(t)$ is the electric field of the pump (a) and probe (b) pulses. We write $\mathbf{E}_j = \lambda_j[\mathbf{e}_j \varepsilon_j(t) + \mathbf{e}_j^* \varepsilon_j^*(t)]$, with \mathbf{e}_j the polarization and $\varepsilon_j(t)$ containing the pulse amplitude, wavevector, and absolute phase. For our purposes, the key feature is the dimensionless λ_j , which scales the amplitude of the pulse. The typical third-order signal derives from a polar-

ization field that is proportional to $\lambda_a^2 \lambda_b$. We define a dimensionless pump intensity $I = \lambda_a^2$.

Moving beyond the lowest-order response, S can be expressed as a power series in I ,

$$S(T, \omega, I) = \overbrace{S^{(3)}(T, \omega)}^{\text{standard TA signal}} I + S^{(5)}(T, \omega) I^2 + S^{(7)}(T, \omega) I^3 + \dots \quad (1)$$

Eq. 1 assumes that the probe is weak and unchanging, and $S^{(n)}$ gives the n^{th} order material response, with only odd orders contributing to TA of samples large enough for phase matching^{16,17}. Standard TA either chooses I small enough that the contributions beyond $S^{(3)}$ are negligible or has the higher-order contributions uncontrollably mixed with the lower-order ones, allowing study of I -dependent trends¹⁸⁻³³. The new HOTA spectroscopy allows separating the $S^{(n)}$ at an intensity I_0 by combining TA spectra taken with N pump intensities

$$I_p = 4I_0 \cos^2 \left(\frac{\pi p}{2N} \right)$$

for $p = 0 \dots N - 1$, where I_0 is chosen so that the contribution from $S^{(2N+3)}$ is negligible. The full method is described in Refs. 13 and 14.

The newly accessible HOTA spectroscopies contain information that has not previously been accessible in TA. This manuscript extends the standard ESA/SE/GSB pathways to higher orders, showing the spectral and dynamical information available in each new order in HOTA. We begin by discussing the dynamical information, which is easier to understand and serves as an intuitive starting place for discussing the higher-order signals. We then describe all of the Liouville pathways that exist for each order, introducing a nomenclature to discuss those contributions that is as useful as ESA/SE/GSB. We then describe the spectral information that exists in each order, focusing on two illustrative model systems.

We make a standard set of assumptions about the systems and light pulses under study. Before the pump arrives, the system is in a thermal state, ρ_{th} . We describe systems – as are commonly discussed in optical spectroscopy – with a ladder of dipole-allowed transitions, where n -

times excited states are distinct from $(n + 1)$ -times excited states, as indicated in the inset of Fig. 1. We use $|n\rangle$ to refer to the set of n -times excited states and use $|n, \nu^{(n)}\rangle$ to refer to a particular state. Such an excitation ladder requires that the states $\{|n, \nu^{(n)}\rangle\}$ are long-lived with respect to the pump pulse duration. If this separation of time scales does not occur, Eq. 1 is still valid, but much of the intuition developed in this paper is not directly applicable.

Each signal $S^{(2n+1)}(T)$ in Eq. 1 can contain the dynamics of at most n -times excited states. This intuitive claim follows from the excitation ladder model and the TA phase-matching condition^{16,34}. We illustrate it using double-sided Feynman diagrams to describe the pathways that contribute to $S^{(2n+1)}$. We assume that the probe is weak, so there is only one interaction with the probe, the remaining $2n$ interactions are with the pump, and the two pulses do not overlap in time. TA phase matching requires that there be equal numbers of left- and right-directed pump interactions, representing the ε_a and ε_a^* terms in the field, and the rotating wave approximation (RWA) requires that arrows directed in cause excitations while arrows directed out cause de-excitations^{16,34}. Then the highest excitation states that can be reached after the pump occur when the raising operator is applied n times to both the bra- and ket-sides of the initial density matrix, which requires $2n$ interactions. We divide the Feynman diagrams into *bases* that involve only interactions with the pump pulse and two *caps* that involve only one interaction with the probe, as shown in Fig. 1, with a full diagram formed by combining any base with either cap. The bases shown in Fig. 1 represent the highest-excitation pathways available at third, fifth, and seventh order. Lower excitation pathways also exist, and we discuss them below. In Fig. 1, the label $|n\rangle \langle m|$ is a placeholder for a density matrix $\sum_{jk} c_{jk} |n, \nu_j^{(n)}\rangle \langle m, \nu_k^{(m)}|$.

We generalize the concept of stimulated emission and excited state absorption from the singly excited states to similar processes that originate from the n -excitation states. When the $S^{(3)}$ bases shown in Fig. 1 are combined with

the absorption (emission) cap we obtain the familiar ESA (SE) pathway. By analogy, when the $S^{(5)}$ bases are combined with the absorption (emission) cap, we obtain a conceptually similar type of signal, which is excited-state absorption or stimulated emission from the doubly excited states. We call these pathways ESA_2/SE_2 for $S^{(5)}$ and ESA_n/SE_n for higher orders. These two pathways contain all of the new dynamical information that is revealed at order $(2n + 1)$. When T is greater than the lifetime of the n -times excited states, the n -times excited population decays during the waiting time, and the ESA_n (SE_n) pathways include absorption (emission) processes beginning from lower-excitation states. Such decays generally change the signal, allowing those lifetimes to be determined¹³. Each HOTA signal also involves contributions from pathways with lower numbers of excitations immediately after the pump. Those pathways have dynamical information that generally already exists in lower-order signals, though interferences of the type discussed below could mask the signal in lower orders. The exception to this rule occurs at third order, where GSB, which is a negation of linear absorption, also introduces ground-state vibrational dynamics that were not present in the static linear absorption signal. As usual, care must be taken in assigning physical significance to pathways. For example, in a two-level system with relaxation, there is no physical excited-state absorption process. However, the ESA pathway must still be calculated, because after the pump pulse excites the system, the system relaxes to the ground state. The probe pulse can then excite the system again. The dynamical information about the lifetime of the excited state is still captured in the SE/ESA pathways.

Since each order controllably adds a single set of excitation states not in the lower-order signals, new dynamics in higher orders can immediately be attributed to new processes. One can analyze each order sequentially, beginning from third order and characterizing the decay constants (e.g., using global analysis^{35–37}) and beat frequencies associated with each order. If the fifth-order signal contains the same decay constants and frequencies as the third-order and

also contains a new set of dynamics, those new dynamics can be attributed to processes involving only the states $|2, \nu^{(2)}\rangle$, and analogously for higher orders.

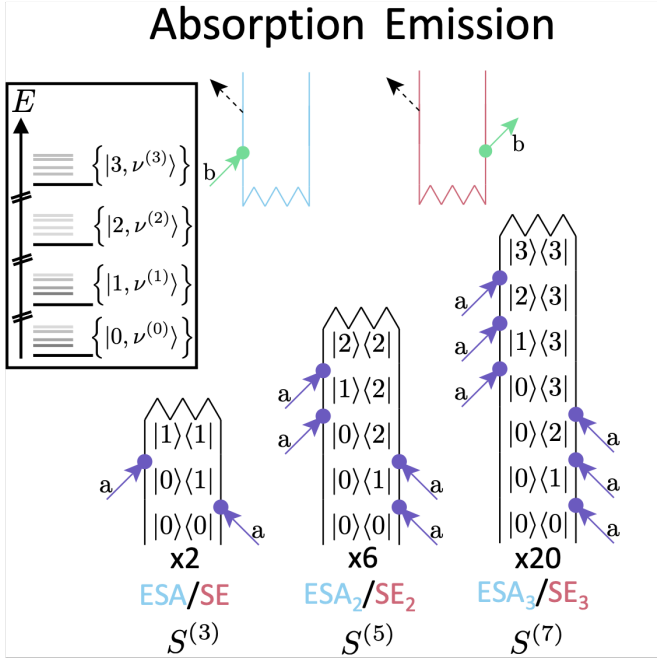


Figure 1: Sample Feynman diagrams for high-order processes broken into *bases* showing the action of the pump pulse, labeled “a”, and *caps* showing the action of the probe pulse, labeled “b”. Each base pairs with each cap, resulting in a complete Feynman diagram. Bases shown produce the highest possible number of excitations at third-, fifth-, and seventh-order, producing the ESA_n/SE_n diagrams with the appropriate cap. The multiplicative number under each base indicates the number of similar bases formed by permutation of the ordering of the pump arrows, confirmed with an automated diagram generator³⁸. The excitation numbers are not shown in the caps, since the caps pair with every base and because n can change due to relaxation during the delay time T . Inset: Sample ladder-type spectrum, with 0-, 1-, 2-, and 3-excitation states shown.

We now consider the full set of pathways contributing to TA signals at all orders. We build up an understanding by comparing the well-known third-order signal to the linear absorption signal (A). Standard third-order TA involves two new processes involving singly ex-

cited states after the pump (ESA/SE) and a negation of the linear absorption (GSB). In order to generalize to higher orders, we also refer to GSB as negated absorption (NA⁽³⁾). This labeling introduces a pattern that applies at higher orders: the $(2n + 1)$ -order signal introduces two new processes (ESA_n/SE_n) and negations of all lower-order processes, which we illustrate in Table 1 and now describe.

Next we compare the fifth- and third-order signals. The fifth-order signal contains new information about the 2-excitation states in the ESA_2/SE_2 pathways shown in Fig. 1. It also includes processes that can be interpreted as negations of the signals associated with the 1-excitation states, which we call negated excited state absorption (NESA) and negated stimulated emission (NSE), shown diagrammatically in Fig. 2. Intuitively these negations occur because the fifth-order response involves moving population from the 1-excitation states that produce ESA/SE to the 2-excitation states as well as back to the 0-excitation states. That increase in ground state population gives an increase in the linear-absorption-type process (undoing part of the GSB), which we call A⁽⁵⁾.

We can extend this pattern and nomenclature to any order, which we demonstrate by comparing the seventh- and fifth-order signals. The new information in seventh order is contained in the ESA_3/SE_3 processes, which report on the 3-excitation states. The seventh-order signal also includes negations of those in the fifth-order pathways, with the relevant bases shown in Fig. 3. The seventh-order signal includes negations of the ESA_2/SE_2 pathways, which we call $NESA_2^{(7)}/NSE_2^{(7)}$, a contribution to the ESA/SE-type processes, which have the same signs as the originals and which we call $ESA^{(7)}/SE^{(7)}$, and a negation of the absorption process, which we call NA⁽⁷⁾.

Each higher-order signal contains pathways that are related to the pathways at the previous order but have opposite signs, as shown on the sub-diagonal of Table 1. We gave the intuitive explanation for these alternating signs; diagrammatically, the alternation can be understood by analyzing the bases in Figs. 1, 2 and 3. Each signal $S^{(2m+1)}$ is proportional to a fac-

tor of $(-i)^{2m+2}$, so every signal order $S^{(2m+1)}$ has an overall factor of $i^2 = -1$ as compared with $S^{(2m-1)}$.¹⁶ In addition, every arrow that occurs on the bra side of the diagrams gives a factor of -1 . Combining these two rules gives the conclusion that ESA_n has the same sign for all n , and similarly that SE_n has the same sign for all n . However, all of the diagrams that correspond to signals that existed in the lower order involve adding an even number of arrows to the bra side of the diagram, as compared to the previous order. Therefore all of these diagrams contribute the opposite sign relative to their previous-order counterparts. The supplementary information contains a discussion of modifications that are required when pump or probe photon energies are close to the thermal energy, e.g., with THz spectroscopies, as well as a discussion of the permutations of the diagrams shown in Figs 1-3.

Table 1: Names of pathways in (transient) absorption spectroscopy to seventh order. The \pm shows the sign of the pathway's contribution. Pathways representing new dynamical information are in bold and appear along the diagonal. Pathways left of the diagonal negate (with the letter N) or revive pathways that first appeared at lower orders. Superscript shows the order of the contribution, which is suppressed for the diagonal contributions

Order	Optical excitations after pump			
	0	1	2	3
1	+ A			
3	-NA ⁽³⁾ (GSB)	+ ESA - SE		
5	+ A ⁽⁵⁾	-NESA ⁽⁵⁾ +NSE ⁽⁵⁾	+ ESA₂ - SE₂	
7	-NA ⁽⁷⁾	+ ESA ⁽⁷⁾ - SE ⁽⁷⁾	-NESA ₂ ⁽⁷⁾ +NSE ₂ ⁽⁷⁾	+ ESA₃ - SE₃

To demonstrate some of the new spectral information present in HOTA, we introduce two model systems. The first is a ladder model with

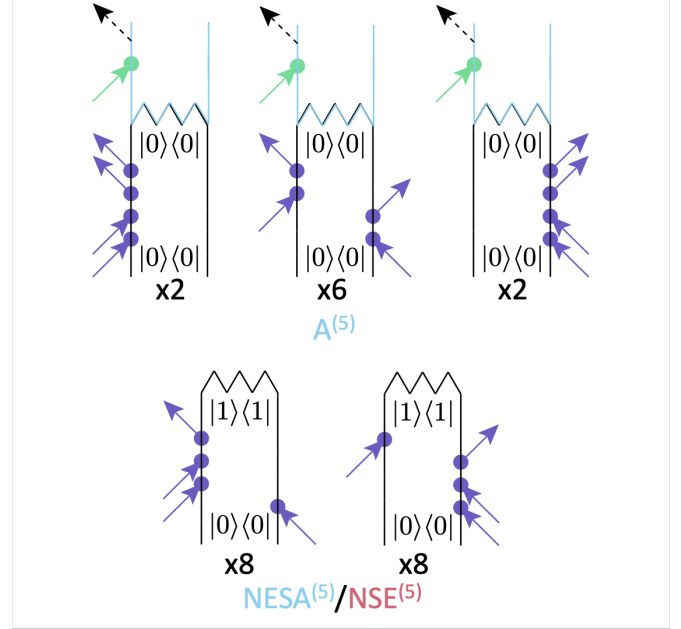


Figure 2: Pathways contributing to $S^{(5)}$ that negate third-order processes. Top row shows contributions to increased ground-state absorption and include the absorption cap. Second row shows bases associated with the negation of the third-order ESA and SE pathways. All 16 bases contribute to NESA⁽⁵⁾ (NSE⁽⁵⁾) when paired with the absorption (emission) cap shown in Fig. 1. The number of similar permutations of the pump interactions is below each diagram. The diagrams associated with ESA_2/SE_2 are displayed in Fig. 1.

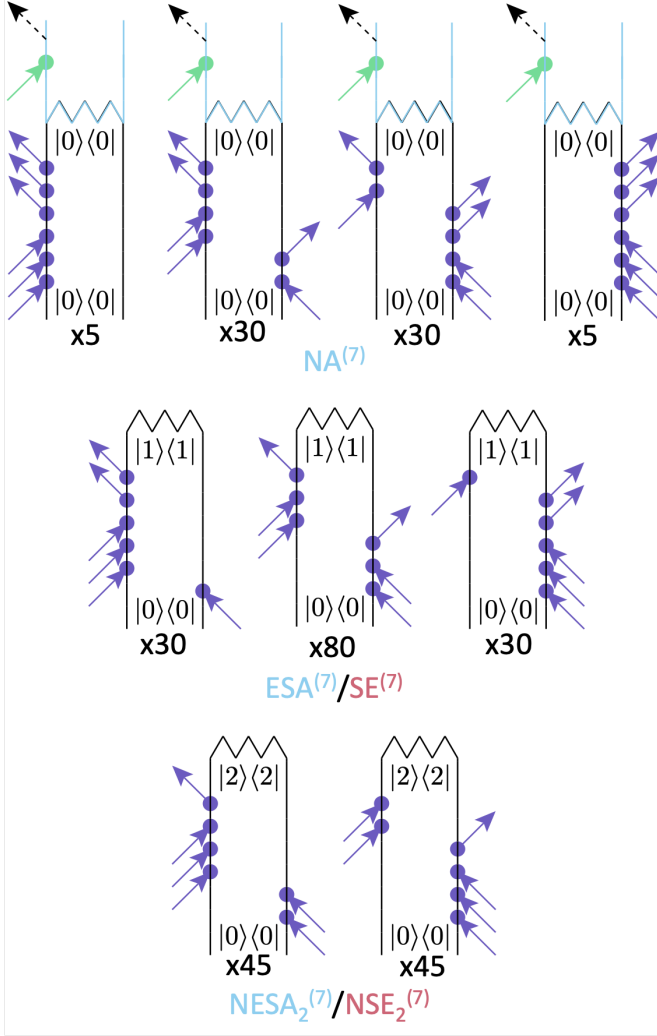


Figure 3: Pathways contributing to $S^{(7)}$ that negate fifth-order processes. Top row shows contributions to negated ground-state absorption and include the absorption cap. Second row shows bases associated with the increase of the third-order ESA and SE processes. Third row shows bases associated with the negation of the fifth-order ESA_2 and SE_2 processes. The number of similar permutations of the pump interactions is below each diagram. The bases associated with ESA_3/SE_3 are displayed in Fig. 1.

Hamiltonian

$$H_0 = \hbar \begin{pmatrix} 0 & 0 & 0 & 0 & 0 \\ 0 & \omega_1 & 0 & 0 & 0 \\ 0 & 0 & \omega_2 & 0 & 0 \\ 0 & 0 & 0 & \omega_3 & 0 \\ 0 & 0 & 0 & 0 & \omega_4 \end{pmatrix}, \quad (2)$$

and dipole operator

$$\mu = \begin{pmatrix} 0 & \mu_{10} & 0 & 0 & 0 \\ \mu_{10} & 0 & \mu_{21} & 0 & 0 \\ 0 & \mu_{21} & 0 & \mu_{32} & 0 \\ 0 & 0 & \mu_{32} & 0 & \mu_{43} \\ 0 & 0 & 0 & \mu_{43} & 0 \end{pmatrix}. \quad (3)$$

We take $\mu_{n,n-k}$ for $k > 1$ to be zero because we assume that the pulse bandwidth does not support such transitions. The frequency differences $\omega_{n,n-1} \equiv \omega_n - \omega_{n-1}$ are the spectral locations where peaks may appear. Note that this excitation ladder model contains no dynamics, so the signal $S^{(2n+1)}$ is constant for $T > 0$, in the impulsive limit. This model could represent an anharmonic vibrational mode of a molecule, which might be studied using IR pump and probe pulses³⁴. The purpose of this discussion is to paint a general picture of the kinds of spectral information that can be revealed (or hidden) in HOTA spectra, regardless of the wavelengths or the sample type.

At each order, new spectral information is revealed by the ESA_n process, which reports on energetic transitions that were inaccessible at the previous order. As long as the new energetic transitions are distinct from previous transitions, this new information appears in spectra as new, positive-signed peaks. To illustrate this idea, we show simulated spectra for an unequally spaced ladder model in Fig. 4, for which we use $\{\omega_1, \omega_2, \omega_3, \omega_4\} = \{1, 1.9, 2.7, 3.4\}\omega_0$ and have assumed that the excitation energies are larger than the thermal energy, with simulations using the open-source ultrafast spectroscopy suite (UFSS)^{38–40}. We take all $\mu_{n,n-1} = 1$ and simulate a closed system with no relaxations, with all of the peaks given the same phenomenological linewidths for visualizing the spectra. The peak at ω_{10} corresponds to linear absorption at first-

order, GSB/SE at third order, and the negations/revivals of these processes at higher orders. The sign of the peak at ω_{10} flips with each order. In addition, each order reveals a new spectral peak, corresponding to ESA at third order and ESA_n at higher-order. Peaks at the same spectral positions appear at higher orders, again with alternating sign.

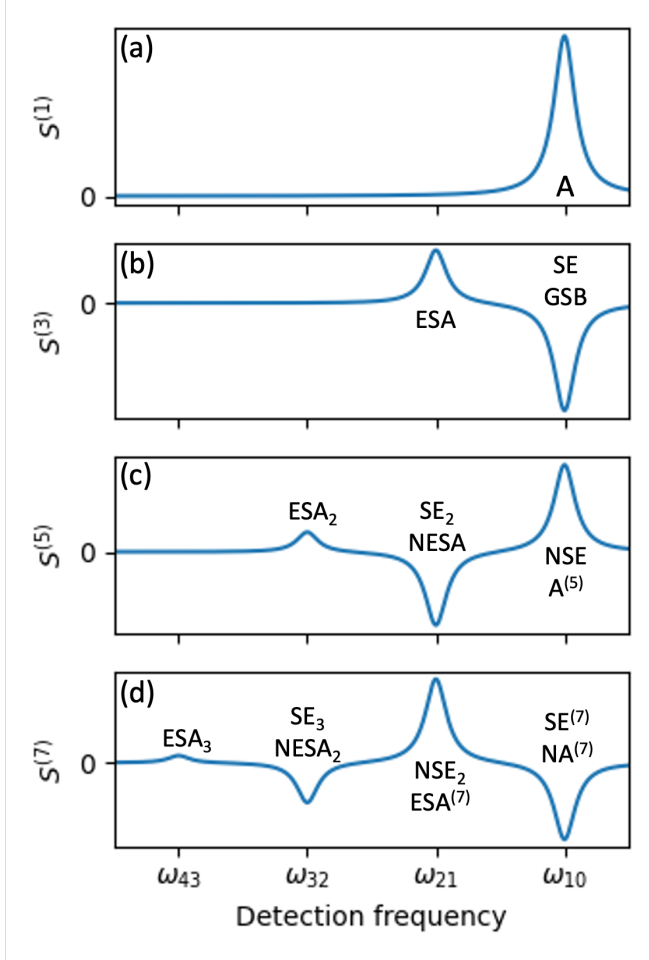


Figure 4: Simulated spectra of an anharmonic ladder for (a) linear absorption (b) standard (third-order) TA, (c) fifth-order TA and (d) seventh-order TA. The ESA_n process is the lowest-energy peak in each spectrum, and always contributes with a positive sign. All spectral features from one spectrum appear with a negative sign in the next spectrum.

When spectral peaks overlap, interpreting the spectra becomes more complicated. To build intuition, we move to a degenerate ladder model in which the ESA_n/SE_n processes are all at the same frequency and allow μ in Eq. 3 to vary. In the supplementary information we derive

expressions for the third- and fifth-order signals, using a model with no 3-excitation states ($\mu_{32} = 0$) and with $\omega_{10} = \omega_{21} = \omega_0$. We see that

$$S^{(3)}(T, \omega_0) \propto -2\mu_{10}^4 + \mu_{21}^2\mu_{10}^2, \quad (4)$$

$$S^{(5)}(T, \omega_0) \propto -\frac{1}{12} (7\mu_{21}^4\mu_{10}^2 - \mu_{21}^2\mu_{10}^4 - 8\mu_{10}^6). \quad (5)$$

In this case, the third-order signal vanishes when $\mu_{21} = \sqrt{2}\mu_{10}$, whereas the fifth-order signal vanishes when $\mu_{21} = \sqrt{8/7}\mu_{10}$, assuming that all processes give the same lineshapes. In the range $\sqrt{8/7} < \mu_{21} < \sqrt{2}$, both the third- and fifth-order signals are negative, breaking the expected pattern of alternating signs that appears in Fig. 4. Note that, for a harmonic vibrational mode, $\mu_{21} = \sqrt{2}\mu_{10}$, and the third-order peak vanishes³. A third-order peak that vanishes due to such interferences between pathways is not unique to vibrational modes, and we demonstrate below how a simple biexciton model may produce the same effect.

If a negative-signed peak appears in both the third- and fifth-order signals at short T , it indicates overlap of transitions to 1- and 2-excitation states. Negative peaks in third-order signals originate in GSB/SE processes between the 0- and 1-excitation states. Looking at Table 1, the only negative contributions to $S^{(5)}$ are SE_2 and $\text{NESA}^{(5)}$, which both occur at the same spectral positions: transitions between 1- and 2-excitation states. The fifth-order negations of the GSB/SE processes have positive sign, so if the fifth-order signal at the same spectral position is also negative, it indicates the presence of a hidden ESA process at third order and indicates that the dipole contributing to that ESA pathway, μ_{21} , cannot be too large. In this case, the fifth-order spectra gives new spectral information about 1-excitation states, as we found in the study of quantum dots in Ref. 13.

As an interesting limiting case, if a peak at some frequency first appears in $S^{(5)}$ and it has a negative amplitude, it reveals a dipole-allowed transition between both $|0\rangle \rightarrow |1\rangle$ and $|1\rangle \rightarrow |2\rangle$ that are normally visible in third order but canceled each other. This situation is in contrast

to a peak that first appears in $S^{(5)}$ with positive sign, which reports on transitions between $|2\rangle$ and $|3\rangle$ states, as discussed above. In our simple model, a new negative peak demonstrates that μ_{21} must be roughly $\sqrt{2}$ stronger than μ_{10} .

This phenomenon of 1-excitation pathways canceling in the third-order signal while appearing in the fifth-order signal can occur in many situations, and we now introduce a model of optical spectroscopy of biexcitons to illustrate another simple case. Let a_A^\dagger and a_B^\dagger create excitons and let the Hamiltonian be

$$H_0 = \hbar \sum_{i=A,B} a_i^\dagger a_i \omega_i + J \left(a_A^\dagger a_B + h.c. \right),$$

where \hbar is Planck's constant and J is the coupling between the two bare excitons with energies $\hbar\omega_i$. The ground-state energy is $\hbar\omega_g = 0$, and the biexciton has energy $\hbar\omega_{AB} = \hbar(\omega_A + \omega_B)$. We set the dipole transitions for each bare exciton equal, that is $\mu_{g,A} = \mu_{g,B} \equiv \mu_0$, and similarly $\mu_{A,AB} = \mu_{B,AB} = \mu_0$, which is different from the previous ladder model, in which the third-order signal vanished only if $\mu_{21} = \sqrt{2}\mu_{10}$. Let $\hbar\omega_\alpha$ and $\hbar\omega_\beta$ be the eigenenergies of the single exciton states, with corresponding transition dipoles $\mu_{g,\alpha}, \mu_{g,\beta}, \mu_{\alpha,AB}$ and $\mu_{\beta,AB}$. Tuning J modifies the single exciton eigenstates and, crucially, $\mu_{g,\alpha}, \mu_{g,\beta}, \mu_{\alpha,AB}$ and $\mu_{\beta,AB}$ ⁴¹.

When the ratio of dipole couplings is correct, the third-order signal at ω_α can be found to cancel, as demonstrated in Fig. 5. When $J = 0.18\hbar(\omega_B - \omega_A)$, the third-order signal at ω_α vanishes, while there is a negative-fifth order signal. As in the ladder model, the new negative feature in the fifth order cannot be an ESA_2 contribution but instead reports on 1-excitation signals that were masked in the third-order. The same phenomenon can also occur in a model with $J = 0$ but fast relaxation from $|B\rangle$ to $|A\rangle$ ¹³. In both realizations of the biexciton model, one of the two exciton peaks is invisible at third-order and appears as a negative peak in the fifth-order signal. The simplicity of the two, quite different, parameter regimes under which this phenomenon appears underscores the fact that this phenomenon can

occur in a wide range of systems.

This discussion emphasizes the value of measuring simultaneously both $S^{(3)}$ and $S^{(5)}$, and shows some of the information that can be revealed by comparing the two signals. We draw particular attention to the fact that comparing the signs of peaks in third- and fifth-order signals immediately reveals the nature of the dominant signal at each spectral location.

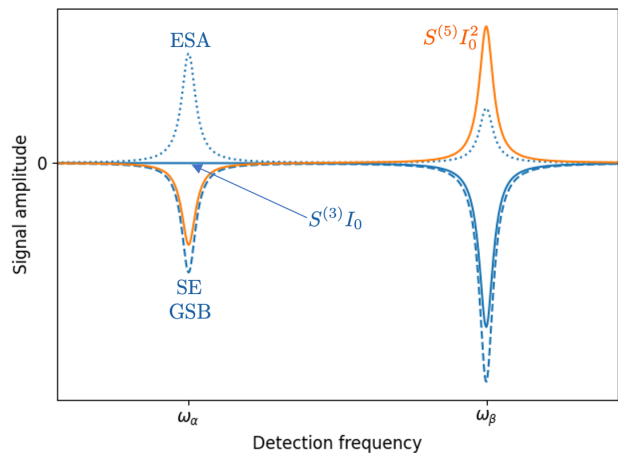


Figure 5: HOTA spectra for a model where the lower exciton peak vanishes at third order (solid blue) and is negative at fifth order (orange). The negative-signed GSB + SE signals (dashed) precisely cancel the positive-signed ESA signal (dotted). Here $J = 0.18(\omega_\beta - \omega_\alpha)$ and there is no relaxation.

Many methods have been used or proposed to extract different high-order responses, frequently involving more than two pulses¹⁵. Refs. 42,43 discuss 3-pulse experiments that are high-order extensions of double-quantum (HODQ) spectroscopy⁴⁴. Both HOTA and HODQ extract the emission/absorption lineshapes for higher lying excited states. HOTA also extracts population dynamics for high-lying excited states. In contrast, HODQ does not extract any population dynamics but rather extracts the frequency-frequency correlation between excitation and emission at a population time of 0. HOTA is experimentally simpler because it requires only a standard TA setup, whereas HODQ requires three pulses and phase-matching or phase-cycling routines. HODQ has the advantage of being background-

free, as there is only a signal if higher-lying excited states exist⁴³. In contrast HOTA always has non-vanishing signals $S^{(2n+1)}$ for all n , even if the system only supports a single dipole-allowed transition. There are also other methods for measuring higher-order responses such as exciton-exciton interaction 2D spectroscopy (EEI2D), a fifth-order signal that gives excitation and emission/absorption lineshapes, as well as population dynamics, but is again more experimentally challenging than HOTA⁴⁵. Both HODQ and EEI2D potentially suffer from higher-order contaminations, which can be difficult to quantify. One of the key advantages offered by HOTA is the clean separation of the nonlinear orders.

We have laid the foundation for understanding the higher-order perturbative terms that can now be measured using the method outlined in Ref. 13. We introduced a language to describe the processes contributing to these higher-order signals and used two simple models to illustrate the new kinds of spectral information that can be uncovered by comparing the third- and fifth-order signals. In particular we showed that new peaks emerging at fifth-order reveal new spectral information if the peak is positive or reveal previously hidden spectral information if the peak is negative. **Acknowledgement**

We acknowledge helpful conversations with Tobias Brixner, Pavel Malý, and Julian Lüttig and a careful reading by Julian Lüttig. We acknowledge funding from the Natural Sciences and Engineering Research Council of Canada.

Supplementary Information

Pump-probe spectroscopy with THz pulses

The expansion in Eq. 1 holds for any wavelengths of the pump and probe beams, and we expect the decomposition technique demonstrated in Ref. 13 to work regardless of wavelength, from THz to xray. In the main text, we work in the limit where the thermal energy is small compared to the laser center frequency of both pump and probe, so that the initial system density matrix exists exclusively in the $|0\rangle$ states. At room temperature, the thermal energy is equivalent to 6 THz. The use of THz probe pulses, in conjunction with IR or optical pump pulses, is a widely used technique^{46,47}, and the use of THz pump pulses is a growing area of research^{27,48,49}. We first discuss the modifications required when using a THz probe and then discuss the more significant changes when using a THz pump, as for rotational spectroscopy. This discussion assumes ambient temperature, but the relevant parameter is the ratio of the photon energy to the thermal energy, and at other temperatures the THz scale should be shifted accordingly.

If the pump central frequency is well above thermal energy (e.g., mid-IR or shorter wavelengths), and the probe pulse is in the THz regime, the interpretations and formalism introduced in the main paper all still apply, but additional Feynman diagrams must be included, which are formed by taking any of the diagrams in Figs. 2 and 3 that end in the states $|0\rangle \langle 0|$ and replacing the absorption cap with the emission cap. These emission-type diagrams occur because, even in the absence of a pump pulse, the probe pulse can stimulate emission from thermally excited populations. Thus the linear response of the system involves not only absorption but also emission, which we call E. Thus there will also be $NE^{(3)}$, $E^{(5)}$ and $NE^{(7)}$ processes at third, fifth and seventh order, respectively, and so on. Figure S1(i) shows a typical ground-state bleach ($NA^{(3)}$) diagram, and Fig. S1(iii) shows the emission ($NE^{(3)}$) counterpart of that diagram. For another example of

an NE⁽³⁾ Feynman diagram, see Fig. 17(viii) of Ref. 50.

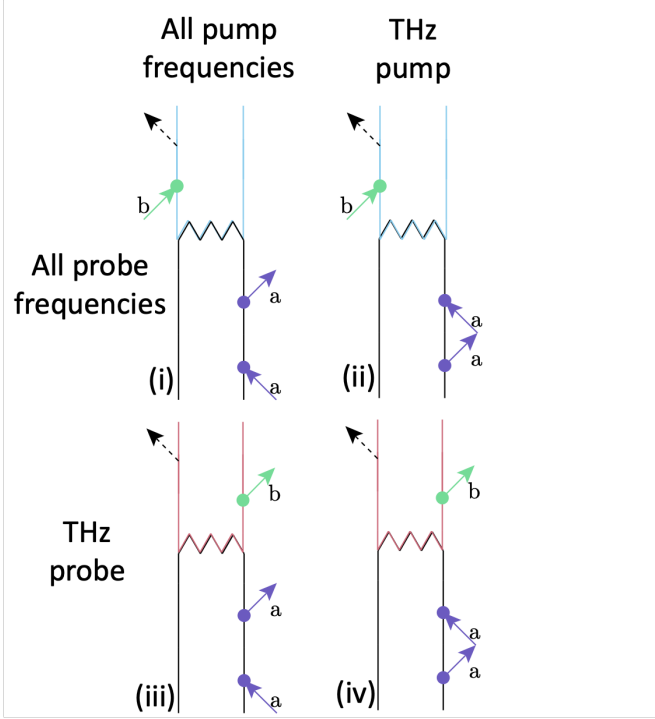


Figure S1: Example diagrams that contribute depending upon the frequencies of the pump and probe pulses: (i) a ground-state bleach diagram that always contributes to TA, (ii) a similar diagram that only contributes when the probe includes THz frequencies, (iii) a permutation of (i) that only contributes when the pump includes THz frequencies, and (iv) a permutation of (iii) that only contributes when both the pump and the probe include THz frequencies.

When the pump central frequency and thermal energy become comparable, the interpretation of HOTA becomes more complicated since the excitation number n (shown schematically in the inset of Fig. 1) cannot be well defined. These complications are similar to those in standard TA interpretation. Depending upon the sensitivity of the experiment, information from the lowest N excitation states is already present in the third-order signal. The initial state of the system is a thermal average over multiple values of n . If we consider a harmonic ladder with frequency ω where $\hbar\omega = k_B T_{sys}$, where k_B is Boltzmann's constant and T_{sys} is the system temperature, then the initial density

matrix $\rho \propto e^{-H/k_B T}$ has $|1\rangle$ states suppressed by a factor of e and $|2\rangle$ states suppressed by a factor of e^2 . The standard third-order TA signal then contains not only the dynamics and spectral features of $|1\rangle$ but also information from $|2\rangle$ that is suppressed by a factor of e and information from $|3\rangle$ that is suppressed by e^2 , and in general information from $|n\rangle$ that is suppressed by a factor of e^{n-1} . If such a third-order experiment can resolve signals up to N excitations, then the fifth-order signal includes information about the lowest $N + 1$ excitation states. Thus we recover an analogous argument to that given in the main text, where each higher order signal adds one new excitation state.

This complication can be seen in the greatly increased number of diagrams that must be considered for the case where $\hbar\omega_{pump} \lesssim k_B T_{sys}$, owing to the thermal average over multiple $|n\rangle$ in the initial thermal state of the system; see Table S1 for the number of diagrams that contribute to various HOTA signals. Figure S1(ii) shows an example of one additional diagram that must be considered, if the pump pulse includes THz frequencies; it is a permutation of a typical ground-state bleach diagram shown in Fig. S1(i), but involves first de-excitation, followed by excitation, of the bra-side of the density matrix. Figure S1(iv) shows an additional diagram that must be considered if both the pump and probe include THz frequencies. For an example of an analogous fifth-order diagram that involves multiple de-excitations, see Fig. 17(xiv) of Ref. 50. The Diagram Generator described in Ref. 38 can be used to visualize all of the diagrams that contribute when the pump and probe pulses both include THz frequencies and can also be used to automate the resulting calculations of the spectra.

While the diagrammatic details are different for THz than they are for optical high-order TA spectroscopy, the main conclusions still hold: higher-order signals give dynamical information about higher excitation states, and each higher order similarly has access to new spectral information.

Table S1: Number of diagrams for calculating HOTA spectra depending upon whether one or both of the pulses is at THz frequencies. In each entry, the numbers given are for third, fifth, and seventh orders, assuming the pump and probe pulses do not overlap in time. Additional diagrams are required if the pulses overlap.

	>THz pump	THz pump
	6	8
>THz probe	54	96
	540	1280
	8	16
THz probe	64	192
	640	2560

Diagram Permutations

Rather than display all of the diagrams, we have displayed representative diagrams in Figures 1, 2, and 3. All of the diagrams contributing to $S^{(3)} - S^{(7)}$ can be obtained from the displayed bases and caps by permuting of the arrows of each base. As an illustration, Fig. S2 shows one permutation of the interactions in an $A^{(5)}$ diagram and one permutation in an $NSE^{(5)}$ diagram, alongside the corresponding diagrams that were displayed in Fig. 2 in the main text. Figure S2 shows permutation of arrows occurring on the same side of the diagram, which show how permuting the interactions on the same side of the diagram can change which transition dipoles contribute to the diagram. In order to obtain all diagrams, one must permute the order of the interactions on opposite sides of the density matrix as well. Such permutations do not change the diagram contributions in the impulsive limit but can change calculations with finite-duration pulses, since different coherences are probed during the pulse duration.

In what we call “Type *a*” diagrams, the system cycles between only the $|0\rangle$ and $|1\rangle$ states, whereas in the “Type *b*” diagrams, the system transitions between the $|0\rangle$, $|1\rangle$, and $|2\rangle$ states.

We note that this taxonomy, with the exception of type *a*, requires a more complicated notation to extend to seventh order and beyond. However, every order has diagrams that could be considered type *a*, which involve only the dipole transition between the $|0\rangle$ and $|1\rangle$ states. Such diagrams offer insight as to why the HOTA signals are non-zero even for a two-level system, where there are no higher-lying excitations present in the system.

The categorization of type *a* and type *b* is also useful in the derivation of the biexciton signal strengths in Eqs. 4 and 5 in the main text. These equations are derived briefly below.

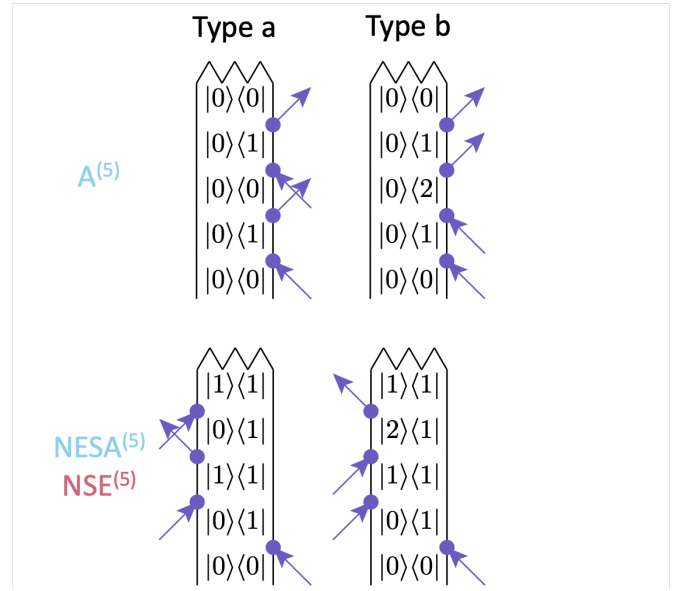


Figure S2: A permutation (left) of the interactions in a base originally shown in Fig. 2 (right). The top row shows two diagrams that contribute to the $A^{(5)}$ pathway, while the bottom row shows two diagrams that contribute to the $NESA^{(5)}/NSE^{(5)}$ pathways.

Optical Biexciton Signal

In Tables S2 and S3 we show the spectral positions and weights for the third- and fifth-order signals, respectively, for a generic ladder model. Adding up the signal contributions from the column “Total weight” gives Eqs. 4 and 5. As described just above, Table S3 distinguishes between *a* pathways, which involve only dipole transitions between the $|0\rangle$ and $|1\rangle$ states during

the pump pulse, and b pathways, which involve dipole transitions between $|0\rangle$, $|1\rangle$, and $|2\rangle$ during the pump pulse, as shown in Fig. S2.

Table S2: Third-order process weights for the ladder model of Eqs. 2, 3.

Process	# of diagrams	Total weight	Spectral position
GSB	2	$-\mu_{10}^4$	ω_{10}
SE	2	$-\mu_{10}^4$	ω_{10}
ESA	2	$+\mu_{21}^2\mu_{10}^2$	ω_{21}

Table S3: Fifth-order diagram weights for the ladder model of Eqs. 2, 3.

Process	# of diagrams	Total weight	Spectral position
$A_a^{(5)}$	8	$+\mu_{10}^6/3$	ω_{10}
$A_b^{(5)}$	2	$+\mu_{21}^2\mu_{10}^4/12$	ω_{10}
NSE_a	8	$+\mu_{10}^6/3$	ω_{10}
NSE_b	8	$+\mu_{21}^2\mu_{10}^4/3$	ω_{10}
$NESA_a$	8	$-\mu_{21}^2\mu_{10}^4/3$	ω_{21}
$NESA_b$	8	$-\mu_{21}^4\mu_{10}^2/3$	ω_{21}
SE_2	6	$-\mu_{21}^4\mu_{10}^2/4$	ω_{21}
ESA_2	6	$+\mu_{32}^2\mu_{21}^2\mu_{10}^2/4$	ω_{32}

References

- (1) Jonas, D. M.; Bradforth, S. E.; Passino, S. A.; Fleming, G. R. Femtosecond Wavepacket Spectroscopy: Influence of Temperature, Wavelength, and Pulse Duration. *The Journal of Physical Chemistry* **1995**, *99*, 2594–2608.
- (2) Berera, R.; van Grondelle, R.; Kennis, J. T. M. Ultrafast Transient Absorption Spectroscopy: Principles and Application to Photosynthetic Systems. *Photosynthesis Research* **2009**, *101*, 105–118.
- (3) Hamm, P. Femtosecond IR Pump-Probe Spectroscopy of Nonlinear Energy Localization in Protein Models and Model Proteins. *Journal of Biological Physics* **2009**, *35*, 17–30.
- (4) Ohkita, H.; Ito, S. Transient Absorption Spectroscopy of Polymer-Based Thin-Film Solar Cells. *Polymer* **2011**, *52*, 4397–4417.
- (5) Cho, B.; Tiwari, V.; Hill, R. J.; Peters, W. K.; Courtney, T. L.; Spencer, A. P.; Jonas, D. M. Absolute Measurement of Femtosecond Pump-Probe Signal Strength. *The Journal of Physical Chemistry A* **2013**, *117*, 6332–6345.
- (6) Maiuri, M.; Garavelli, M.; Cerullo, G. Ultrafast Spectroscopy: State of the Art and Open Challenges. *Journal of the American Chemical Society* **2019**,
- (7) Pandya, R.; Chen, R. Y. S.; Gu, Q.; Gorman, J.; Auras, F.; Sung, J.; Friend, R.; Kukura, P.; Schnedermann, C.; Rao, A. Femtosecond Transient Absorption Microscopy of Singlet Exciton Motion in Side-Chain Engineered Perylene-Diimide Thin Films. *The Journal of Physical Chemistry A* **2020**, *124*, 2721–2730.
- (8) Provazza, J.; Segatta, F.; Coker, D. F. Modeling Nonperturbative Field-Driven Vibronic Dynamics: Selective State Preparation and Nonlinear Spectroscopy. *Journal of Chemical Theory and Computation* **2021**, *17*, 29–39.
- (9) Cina, J. A. In *Getting Started on Time-Resolved Molecular Spectroscopy*; Cina, J. A., Ed.; Oxford University Press, 2022; p 0.
- (10) Xu, C.; Lin, K.; Hu, D.; Gu, F. L.; Gelin, M. F.; Lan, Z. Ultrafast Internal Conversion Dynamics through the On-the-Fly Simulation of Transient Absorption Pump-Probe Spectra with Different

- Electronic Structure Methods. *The Journal of Physical Chemistry Letters* **2022**, *13*, 661–668.
- (11) Unger, F.; Moretti, L.; Hausch, J.; Bredehoeft, J.; Zeiser, C.; Haug, S.; Tempelaar, R.; Hestand, N. J.; Cerullo, G.; Broch, K. Modulating Singlet Fission by Scanning through Vibronic Resonances in Pentacene-Based Blends. *Journal of the American Chemical Society* **2022**, *144*, 20610–20619.
- (12) Sayer, T.; Farah, Y. R.; Austin, R.; Sambur, J.; Krummel, A. T.; Montoya-Castillo, A. Trion Formation Resolves Observed Peak Shifts in the Optical Spectra of Transition-Metal Dichalcogenides. *Nano Letters* **2023**, *23*, 6035–6041.
- (13) Malý, P.; Lüttig, J.; Rose, P. A.; Turkin, A.; Lambert, C.; Krich, J. J.; Brixner, T. Separating Single- from Multi-Particle Dynamics in Nonlinear Spectroscopy. *Nature* **2023**, *616*, 280–287.
- (14) Lüttig, J.; Rose, P. A.; Malý, P.; Turkin, A.; Bühler, M.; Lambert, C.; Krich, J. J.; Brixner, T. High-Order Pump–Probe and High-Order Two-Dimensional Electronic Spectroscopy on the Example of Squaraine Oligomers. *The Journal of Chemical Physics* **2023**, *158*, 234201.
- (15) Lüttig, J.; Mueller, S.; Malý, P.; Krich, J. J.; Brixner, T. Higher-Order Multidimensional and Pump–Probe Spectroscopies. *The Journal of Physical Chemistry Letters* **2023**, *14*, 7556–7573.
- (16) Mukamel, S. *Principles of Nonlinear Optical Spectroscopy*; Oxford Series in Optical and Imaging Sciences; Oxford University Press: Oxford, New York, 1999.
- (17) Boyd, R. W. In *Nonlinear Optics*; Boyd, R. W., Ed.; Academic Press: Burlington, 2008.
- (18) Auston, D. H.; Shank, C. V.; LeFur, P. Picosecond Optical Measurements of Band-to-Band Auger Recombination of High-Density Plasmas in Germanium. *Physical Review Letters* **1975**, *35*, 1022–1025.
- (19) Pedersen, S.; Baumert, T.; Zewail, A. H. Femtosecond Real-Time Probing of Reactions. 13. Multiphoton Dynamics of Mercury Iodide (IHgI). *The Journal of Physical Chemistry* **1993**, *97*, 12460–12465.
- (20) Bittner, T.; Irrgang, K.-D.; Renger, G.; Wasielewski, M. R. Ultrafast Excitation Energy Transfer and Exciton-Exciton Annihilation Processes in Isolated Light Harvesting Complexes of Photosystem II (LHC II) from Spinach. *The Journal of Physical Chemistry* **1994**, *98*, 11821–11826.
- (21) Smith, G. O.; Mayer, E. J.; Kuhl, J.; Ploog, K. Pump-Probe Investigations of Biexcitons in GaAs Quantum Wells. *Solid State Communications* **1994**, *92*, 325–329.
- (22) Valkunas, L.; Trinkunas, G.; Liuolia, V.; van Grondelle, R. Nonlinear Annihilation of Excitations in Photosynthetic Systems. *Biophysical Journal* **1995**, *69*, 1117–1129.
- (23) Yokoyama, K.; Silva, C.; Son, D. H.; Walhout, P. K.; Barbara, P. F. Detailed Investigation of the Femtosecond Pump-Probe Spectroscopy of the Hydrated Electron. *The Journal of Physical Chemistry A* **1998**, *102*, 6957–6966.
- (24) Klimov, V. I.; Mikhailovsky, A. A.; McBranch, D. W.; Leatherdale, C. A.; Bawendi, M. G. Quantization of Multiparticle Auger Rates in Semiconductor Quantum Dots. *Science* **2000**, *287*, 1011–1013.
- (25) Brüggemann, B.; May, V. Exciton Exciton Annihilation Dynamics in Chromophore Complexes. II. Intensity Dependent Transient Absorption of the LH2 Antenna System. *The Journal of Chemical Physics* **2004**, *120*, 2325–2336.

- (26) Ueda, A.; Matsuda, K.; Tayagaki, T.; Kanemitsu, Y. Carrier Multiplication in Carbon Nanotubes Studied by Femtosecond Pump-Probe Spectroscopy. *Applied Physics Letters* **2008**, *92*, 233105.
- (27) Hoffmann, M. C.; Hebling, J.; Hwang, H. Y.; Yeh, K.-L.; Nelson, K. A. THz-pump/THz-probe Spectroscopy of Semiconductors at High Field Strengths [Invited]. *JOSA B* **2009**, *26*, A29–A34.
- (28) Taguchi, S.; Saruyama, M.; Teranishi, T.; Kanemitsu, Y. Quantized Auger Recombination of Biexcitons in CdSe Nanorods Studied by Time-Resolved Photoluminescence and Transient-Absorption Spectroscopy. *Physical Review B* **2011**, *83*, 155324.
- (29) Almand-Hunter, A. E.; Li, H.; Cundiff, S. T.; Mootz, M.; Kira, M.; Koch, S. W. Quantum Droplets of Electrons and Holes. *Nature* **2014**, *506*, 471–475.
- (30) Chlouba, T.; Trojánek, F.; Kopecký, V., Jr.; López-Vidrier, J.; Hernández, S.; Hiller, D.; Gutsch, S.; Zacharias, M.; Malý, P. Pathways of Carrier Recombination in Si/SiO₂ Nanocrystal Superlattices. *Journal of Applied Physics* **2019**, *126*, 163101.
- (31) Soni, A.; Kushavah, D.; Lu, L.-S.; Chang, W.-H.; Pal, S. K. Ultrafast Exciton Trapping and Exciton–Exciton Annihilation in Large-Area CVD-Grown Monolayer WS₂. *The Journal of Physical Chemistry C* **2021**, *125*, 23880–23888.
- (32) Navotnaya, P.; Sohoni, S.; Lloyd, L. T.; Abdulhadi, S. M.; Ting, P.-C.; Higgins, J. S.; Engel, G. S. Annihilation of Excess Excitations along Phycocyanin Rods Precedes Downhill Flow to Allophycocyanin Cores in the Phycobilisome of *Synechococcus Elongatus* PCC 7942. *The Journal of Physical Chemistry B* **2022**, *126*, 23–29.
- (33) Kumar, S.; Dunn, I. S.; Deng, S.; Zhu, T.; Zhao, Q.; Williams, O. F.; Tempelaar, R.; Huang, L. Exciton Annihilation in Molecular Aggregates Suppressed through Quantum Interference. *Nature Chemistry* **2023**, *15*, 1118–1126.
- (34) Hamm, P.; Zanni, M. *Concepts and Methods of 2D Infrared Spectroscopy*; Cambridge University Press: Cambridge, 2011.
- (35) Knutson, J. R.; Beechem, J. M.; Brand, L. Simultaneous Analysis of Multiple Fluorescence Decay Curves: A Global Approach. *Chemical Physics Letters* **1983**, *102*, 501–507.
- (36) Steinbach, P. J.; Ionescu, R.; Matthews, C. R. Analysis of Kinetics Using a Hybrid Maximum-Entropy/Nonlinear-Least-Squares Method: Application to Protein Folding. *Biophysical Journal* **2002**, *82*, 2244–2255.
- (37) van Stokkum, I. H. M.; Larsen, D. S.; van Grondelle, R. Global and Target Analysis of Time-Resolved Spectra. *Biochimica et Biophysica Acta (BBA) - Bioenergetics* **2004**, *1657*, 82–104.
- (38) Rose, P. A.; Krich, J. J. Automatic Feynman Diagram Generation for Nonlinear Optical Spectroscopies and Application to Fifth-Order Spectroscopy with Pulse Overlaps. *The Journal of Chemical Physics* **2021**, *154*, 034109.
- (39) Rose, P. A.; Krich, J. J. Numerical Method for Nonlinear Optical Spectroscopies: Ultrafast Ultrafast Spectroscopy. *The Journal of Chemical Physics* **2019**, *150*, 214105.
- (40) Rose, P. A.; Krich, J. J. Efficient Numerical Method for Predicting Nonlinear Optical Spectroscopies of Open Systems. *The Journal of Chemical Physics* **2021**, *154*, 034108.
- (41) Yuen-Zhou, J.; Krich, J. J.; Kassal, I.; Johnson, A. S.; Aspuru-Guzik, A. *Ultra-*

fast Spectroscopy: Quantum Information and Wavepackets; IOP Publishing, 2014.

Physical Chemistry Chemical Physics **2022**, *24*, 653–665.

- (42) Yu, S.; Titze, M.; Zhu, Y.; Liu, X.; Li, H. Observation of Scalable and Deterministic Multi-Atom Dicke States in an Atomic Vapor. *Optics Letters* **2019**, *44*, 2795–2798.
- (43) Abramavičius, D. Revealing a Full Quantum Ladder by Nonlinear Spectroscopy. *Lithuanian Journal of Physics* **2020**, *60*.
- (44) Yang, L.; Mukamel, S. Revealing Exciton-Exciton Couplings in Semiconductors Using Multidimensional Four-Wave Mixing Signals. *Physical Review B* **2008**, *77*, 075335.
- (45) Malý, P.; Lüttig, J.; Turkin, A.; Dostál, J.; Lambert, C.; Brixner, T. From Wavelike to Sub-Diffusive Motion: Exciton Dynamics and Interaction in Squaraine Copolymers of Varying Length. *Chemical Science* **2020**, *11*, 456–466.
- (46) George, P. A.; Strait, J.; Dawlaty, J.; Shivaraman, S.; Chandrashekar, M.; Rana, F.; Spencer, M. G. Ultrafast Optical-Pump Terahertz-Probe Spectroscopy of the Carrier Relaxation and Recombination Dynamics in Epitaxial Graphene. *Nano Letters* **2008**, *8*, 4248–4251.
- (47) Xiao, Z.; Wang, J.; Liu, X.; Assaf, B. A.; Burghoff, D. Optical-Pump Terahertz-Probe Spectroscopy of the Topological Crystalline Insulator $\text{Pb}_{1-x}\text{Sn}_x\text{Se}$ through the Topological Phase Transition. *ACS Photonics* **2022**, *9*, 765–771.
- (48) Lu, J.; Zhang, Y.; Hwang, H. Y.; Ofori-Okai, B. K.; Fleischer, S.; Nelson, K. A. Nonlinear Two-Dimensional Terahertz Photon Echo and Rotational Spectroscopy in the Gas Phase. *Proceedings of the National Academy of Sciences* **2016**, *113*, 11800–11805.
- (49) Novelli, F.; Hoberg, C.; Adams, E. M.; Klopff, J. M.; Havenith, M. Terahertz Pump–Probe of Liquid Water at 12.3 THz.
- (50) Lu, J.; Li, X.; Zhang, Y.; Hwang, H. Y.; Ofori-Okai, B. K.; Nelson, K. A. Two-Dimensional Spectroscopy at Terahertz Frequencies. *Topics in Current Chemistry* **2018**, *376*, 6.